ADVANCED FUNCTIONAL MATERIALS
www.afm-journal.de

Liquid-Metal Electrode for High-Performance Triboelectric Nanogenerator at an Instantaneous Energy Conversion Efficiency of 70.6%

Wei Tang, Tao Jiang, Feng Ru Fan, Ai Fang Yu, Chi Zhang, Xia Cao, and Zhong Lin Wang**

Harvesting ambient mechanical energy is a key technology for realizing self-powered electronics, which has tremendous applications in wireless sensing networks, implantable devices, portable electronics, etc. The currently reported triboelectric nanogenerator (TENG) mainly uses solid materials, so that the contact between the two layers cannot be 100% with considering the roughness of the surfaces, which greatly reduces the total charge density that can be transferred and thus the total energy conversion efficiency. In this work, a liquid-metal-based triboelectric nanogenerator (LM-TENG) is developed for high power generation through conversion of mechanical energy, which allows a total contact between the metal and the dielectric. Due to that the liquid–solid contact induces large contacting surface and its shape adaptive with the polymer thin films, the LM-TENG exhibits a high output charge density of 430 μC m^{-2}, which is four to five times of that using a solid thin film electrode. And its power density reaches 6.7 W m^{-2} and 133 kW m^{-3}. More importantly, the instantaneous energy conversion efficiency is demonstrated to be as high as 70.6%. This provides a new approach for improving the performance of the TENG for special applications. Furthermore, the liquid easily fluctuates, which makes the LM-TENG inherently suitable for vibration energy harvesting.

1. Introduction

With the rapid increasing of portable electronics and wireless sensing networks, scavenging ambient mechanical energy as a sustainable power source for powering these devices is a focus of today's research. Various approaches based on piezoelectric,[1–4] electromagnetic,[5,6] electrostatic effects[7–10] have been demonstrated. Besides, many novel liquid-based energy conversion technologies, including reverse electrowetting[11] and electric-double-layer modulating[12] are also proposed. Recently, by combining triboelectric effect[13,14] and the electrostatic induction phenomenon, triboelectric nanogenerator (TENG) is invented. It features in low cost, diversiform material options, and free of pre-charging, and shows a significantly high power output and a high energy conversion efficiency up to 55%.[15–18] Therefore, it enables self-powered, autonomous electronics and potentially large-scale power generation possible.[19,20] However, all of the TENGs reported today are normally based on solid materials, so that the effectiveness of contact, especially to the nanometer level, can be largely affected by the roughness of the two surfaces and the match between the two. According to the literature, the present TENG's charge density is about 100 μC m^{-2}.[21,22] Meanwhile, the solid–solid friction will result in heat generation and dissipation. Those two largely limit the efficiency of the TENG.

The current mostly used low-cost electrodes are aluminum and copper. As a metal material, liquid metal is widely investigated for its outstanding physical capabilities,[23,24] such as high conductivity and favorable flexibility, which initiates promising applications in chip cooling,[25] printed electronics,[26,27] and energy science (lithium battery,[28] thermoelectric cell).[29] Since triboelectrification is a surface charging effect[14,30] and the liquid–solid contact will potentially introduce larger contact area, higher contact intimacy, and lower friction coefficient, with respect to the solid–solid contact, the liquid metal would be an ideal contact material for TENG's contact electrode.

In this work, we develop the liquid-metal-based triboelectric nanogenerator (LM-TENG). Operating at a separating velocity of 0.25 m s^{-1}, the LM-TENG having a contact area of 15 cm^2 could generate a voltage of 679 V and a current of 9 μA. More importantly, its output charge density reaches 430 μC m^{-2},

Dr. W. Tang, Dr. T. Jiang, Dr. F. R. Fan, Dr. A. F. Yu, Dr. C. Zhang, Prof. X. Cao, Prof. Z. L. Wang
Beijing Institute of Nanoenergy and Nanosystems
Chinese Academy of Sciences
Beijing 100083, China
E-mail: caoxia@ustb.edu.cn; zlwang@gatech.edu
Prof. X. Cao
School of Chemistry and Biological Engineering
University of Science and Technology Beijing
Beijing 100083, China
Prof. Z. L. Wang
School of Material Science and Engineering
Georgia Institute of Technology
Atlanta, GA 30332-0245, USA

DOI: 10.1002/adfm.201501331

which is over four times higher than that of the solid–solid-contact TENG, and its power density reaches 6.7 W m^{-2} and 133 kW m^{-3}. Owing to the shape-adaptive advantage, with a 20-layer configuration, the LM-TENG achieves a high current output above 130 μA. In addition, the liquid-metal-based TENG's energy conversion efficiency is demonstrated to be 70.6%, even higher than the previous reported 55%. Furthermore, the LM-TENG is applied for vibration energy harvesting. At amplitude of 1.2 mm and a frequency of 10 Hz, the LM-TENG outputs a voltage of 145 V, a current of 5.8 μA, and charges a 100 μF capacitor to 1 V in 65 s. This work presents a new approach for enhancing the TENG's output performance and further broadening its applications.

2. Liquid-Metal Triboelectric Nanogenerator

In this work, the output voltage and current of the LM-TENG are measured using a digital oscilloscope from Agilent with its inner impedance of 100 MΩ and an SR570 low noise current amplifier from Stanford Research Systems, respectively.

2.1. Device Configuration and Working Principle

A LM-TENG is composed of two parts, as schemed in **Figure 1**a. One part is a slice, composed of friction material and its induction electrode, and the other is the liquid metal. The friction material could be any insulating material with different electron-attractive ability compared to the liquid metal, such as polyimide (Kapton), polytetrafluoroethylene (PTFE), polyethylene terephthalate (PET), and so on. The induction electrode's one end is fully covered by the friction material, avoiding any shortcut between the induction electrode and the liquid metal. As for the liquid metal, many choices are valid, including mercury, gallium, etc.

Figure 1b depicts the working principle of the LM-TENG step by step, which can be explained as a result of triboelectrification and electrostatic induction. When the slice is partly immersed into the liquid metal, the friction material makes contact with the liquid metal. According to the literature,[15,16] due to their different abilities in attracting electrons, the electrons will be injected from the liquid metal to the surface of the friction layer, so that there will be net negative charges on the surface of the friction layer and net positive charges on the interface of the liquid metal (Figure 1b(i)). As the slice moves out of the liquid, the tribocharges in the interface regions are separated, which will induce a higher potential in the liquid metal than the induction electrode; thus the electrons in the induction electrode will be driven to flow to the liquid metal through an external load (form a current flow in the reverse direction, Figure 1b(ii)). In this process, electrons keep flowing until the slice is fully taken out, which is represented by Figure 1b(iii). At this moment, both the induced potential difference and the amount of transferred charges between the induction electrode and the liquid metal reach the maximum values. As the slice moves back into the liquid metal, the potential difference will drop with the increase of the slice's wetting area. As a result, the electrons will flow back in the opposite direction from the liquid metal to the induction electrode (Figure 1b(iv)). Thus, the entire process will result in an AC pulse output.

2.2. Characterization of the LM-TENG

The electric characteristics of the LM-TENG are measured at the slice's moving velocity of 0.25 m s^{-1}. The Kapton (50 μm thick), copper, and mercury serve as the friction material, induction electrode, and liquid metal, respectively. The measured results of the open-circuit voltage (V_{oc}), short-circuit current (I_{sc}), and amount of transferred charges (Q) are displayed in **Figure 2**a–c. It can be observed that the LM-TENG can deliver a high output performance as V_{oc} = 679 V, I_{sc} = 9 μA, and Q = 0.645 μC. Taking the contacting area of 15 cm^2 into account, the output charge density reaches 430 μC m^{-2}, which is much higher than the previous solid–solid contact-induced charge density that is around 100 μC m^{-2}.[21,22] The output current is also measured with different resistances connected in the load. It remains stable when the resistance is smaller than 100 MΩ and then decreases as the resistance increases. An optimum output power of 10 mW (6.7 W m^{-2} and 133 kW m^{-3}) is delivered at a resistance of 1 GΩ (Figure 2d).

2.3. Materials Dependence of the LM-TENG

To further demonstrate the concept of the liquid-metal-based TENG, gallium is utilized (purity 99.999%). After placing in a tank filled with 50 °C hot water, the gallium melts. By using the similar experiment setup (a 50 μm thick Kapton serves as the friction material, with a contacting area of 6 cm^2), the gallium-based TENG is examined and compared with the mercury-based TENG (**Figure 3**a,b). It shows that the gallium-based TENG definitely works, suggesting that any other liquid metal could be utilized, such as galinstan, which is commercial. As for the output performance, the maximum output voltage and current

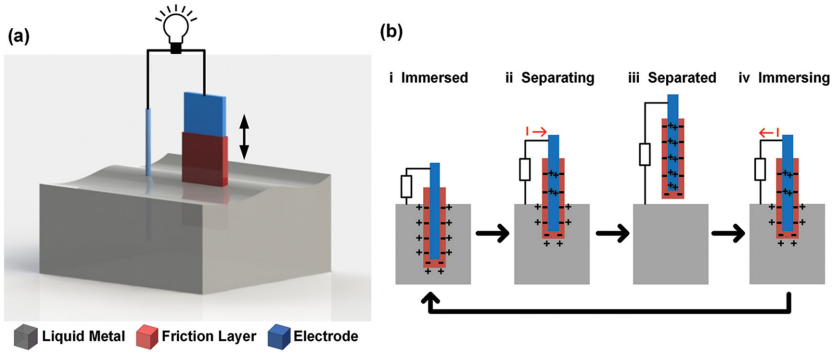

Figure 1. Working principle of the liquid-metal-based triboelectric nanogenerator. a) Schematic illustration showing the device configuration of the LM-TENG. b) Step-by-step illustration showing the working principle of the LM-TENG.

Adv. Funct. Mater. 2015,
DOI: 10.1002/adfm.201501331

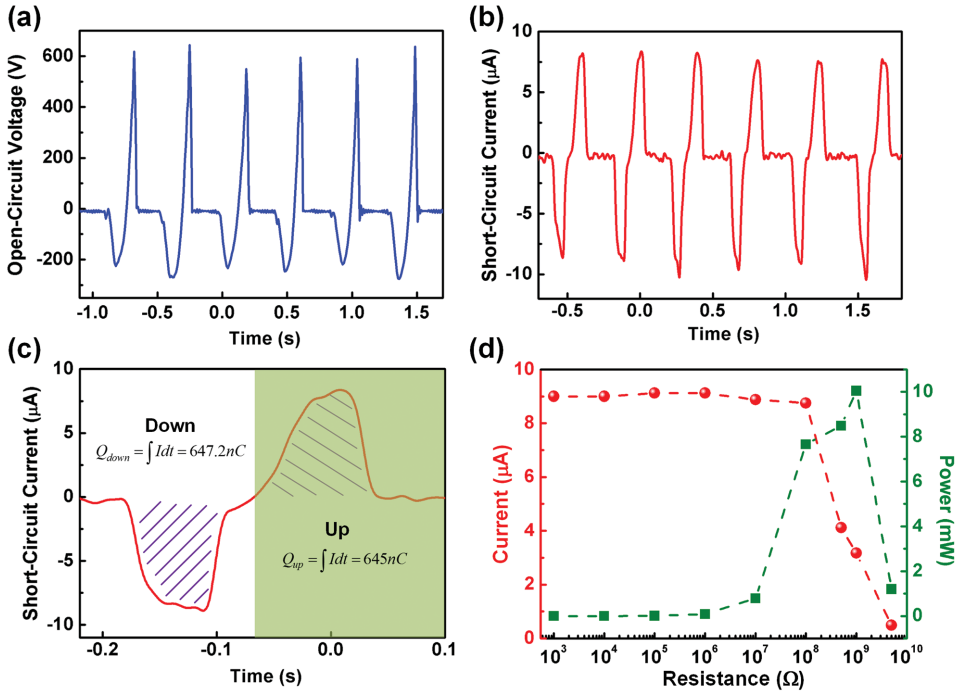

Figure 2. Electric characteristics of the mercury-based TENG with 50 μm thick Kapton as the friction material. a–c) Measurement results of the open-circuit voltage, short-circuit current, and transferred charges of the TENG, respectively. d) Output current and power under variable load resistances.

of the gallium-based TENG are around 50 V and 0.66 μA, which are, respectively, 12.5% and 13.8% of that of the mercury-based TENG. By integrating the curve of I_{SC}, it can be found that the mercury-based TENG can provide a charge amount of 250.1 nC and a charge density of 416.8 μC m^{-2}, corresponding with our above test. Whereas, those of gallium-based TENG are much

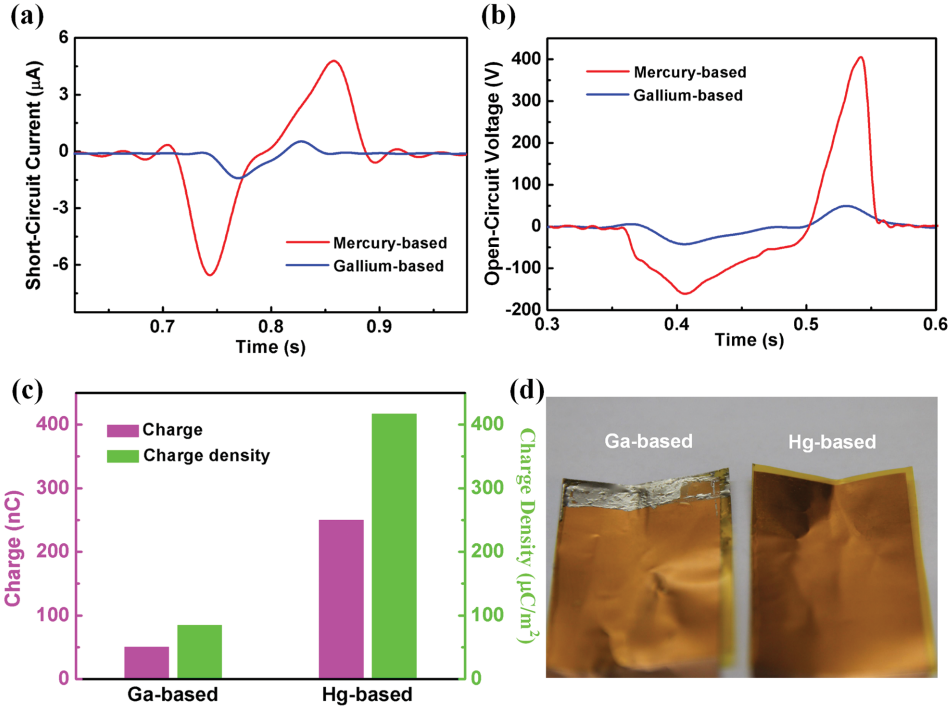

Figure 3. Principle demonstration in another liquid metal—gallium. a–c) Comparisons of the gallium-based and mercury-based TENGs' performances on the open-circuit voltage, short-circuit current, transferred charge, and charge density. d) Optical images of the Kapton surfaces after immersed in gallium and mercury, respectively.

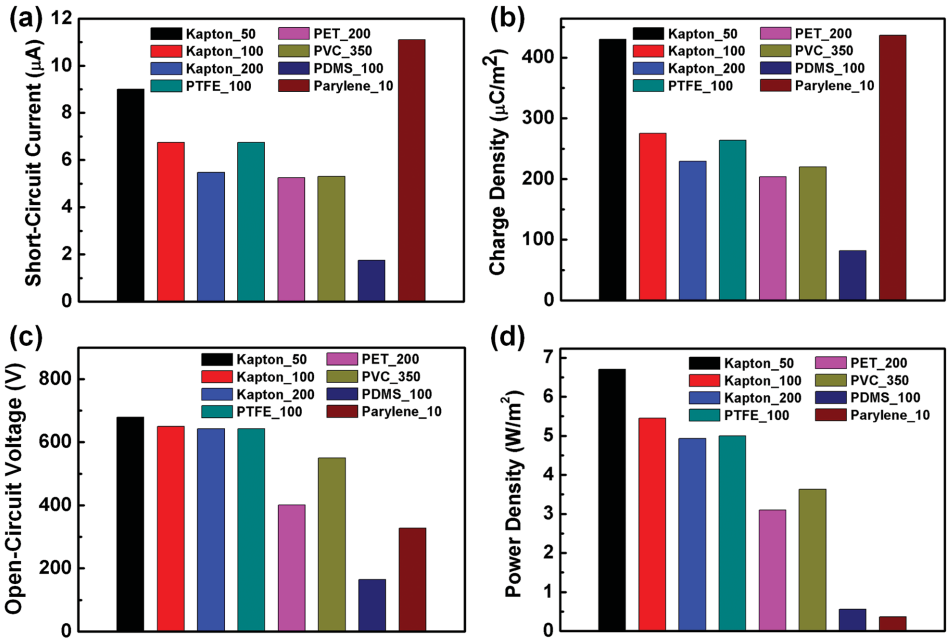

Figure 4. Dependences of the output performance of the LM-TENG on various friction materials. Friction materials' impact on a) the open-circuit voltage, b) the short-circuit current, c) the transferred charge density, and d) the output power density.

smaller, i.e., 50.7 nC and 84.5 μC m^{-2} (Figure 3c). This is because the gallium's surface gets oxidized instantaneously, when it is exposed to the ambient air, which makes it as if a gel rather than a normal liquid,[31] and thus some gallium or gallium oxide remains on the Kapton's surface even after the slice is separated from the liquid (Figure 3d), resulting in a partial screening of the tribocharges. Consequently, smaller electrical outputs are obtained. Considering this, oxygen-free encapsulation will solve this problem.[31] In this work, our following tests are therefore simply based on mercury.

Subsequently, we measure the LM-TENG's output performance based on various friction materials, including Kapton, PTFE, PET, polyvinyl chloride, polydimethylsiloxane (PDMS), and parylene. Their contacting areas are all set at 15 cm^2 and the thicknesses are appended right after its name, with the unit of micro meter. Measurement results are plotted in **Figure 4**.

It can be seen from the case of Kaptons, the film thickness has a significant influence on the TENG's output, especially in the output current and charge density. As the Kapton thickness increases from 50 to 200 μm, the LM-TENG's output current decreases from 9 to 5.47 μA (Figure 4a) and the charge density descents from 430 μC m^{-2} to 229 μC m^{-2} (Figure 4b). According to the literature, it is due to the increase of the induction distance.[32] In addition, the output voltage is also lowered (Figure 4c) as well as the output power (Figure 4d).

From Figure 4b, the triboelectrification-induced charge series can also be obtained. Set at the same thickness (100 μm), PTFE outputs almost the same charge density as Kapton and obviously larger than PDMS. If the thickness is 200 μm, PET exhibits a lower charge density with respect to Kapton but higher than 100 μm thick PDMS. Therefore, a triboelectric series for these materials can be concluded as Kapton ≈ PTFE > PET > PDMS, which corresponds to the previous work[15] to some degree, except for PDMS. This is explained as that the plane PDMS's surface is so sticky that the mercury residuum attached on the surface (Figure S1, Supporting Information). It results in a partial screening effect, similar to the gallium-based TENG.

Furthermore, it is worth noting that when the friction material is parylene, the TENG shows a high current and a medium voltage, but its effective output power is rather low. We compare the electrical output of the parylene-based LM-TENG with that of the Kapton-based one, upon connecting to different resistances (Figure S2, Supporting Information). It is found that the current of the parylene-based LM-TENG starts to descent when the resistance is 1 MΩ; alternatively, the Kapton-based one starts decreasing when the resistance reaches 100 MΩ. Finally, the matched resistances for the two types of TENGs are 100 MΩ and 1 GΩ, respectively. As a consequence, the maximum power output of the parylene-based LM-TENG is lower.

2.4. Surface Morphology Influence on the LM-TENG

Triboelectrification is a surface charging effect, so that the output current and charge of the TENG are expected to linearly scale with the contacting area between the two materials.[33] Since liquid is shape adaptive, it is promising to employ a large specific surface to enhance the LM-TENG's output performance. Herein, we compare four surface morphologies with different depth-to-diameter ratios, as shown in **Figure 5**a. They are all made of aluminum sheet, with an array of cylinders structures on the surface. These cylinders are 1 mm in thickness, and 4, 2, and 1 mm, respectively, in both diameter and spacing (The first type is the plane structure with its depth-to-diameter defined as 0). Then, the four sheets are all covered by a layer of 10 μm thick parylene deposited by vacuum vapor deposition.

Testing results reveal that higher specific surface results in higher output current and charges (Figure 5b,c). However, as the

Adv. Funct. Mater. **2015**,
DOI: 10.1002/adfm.201501331

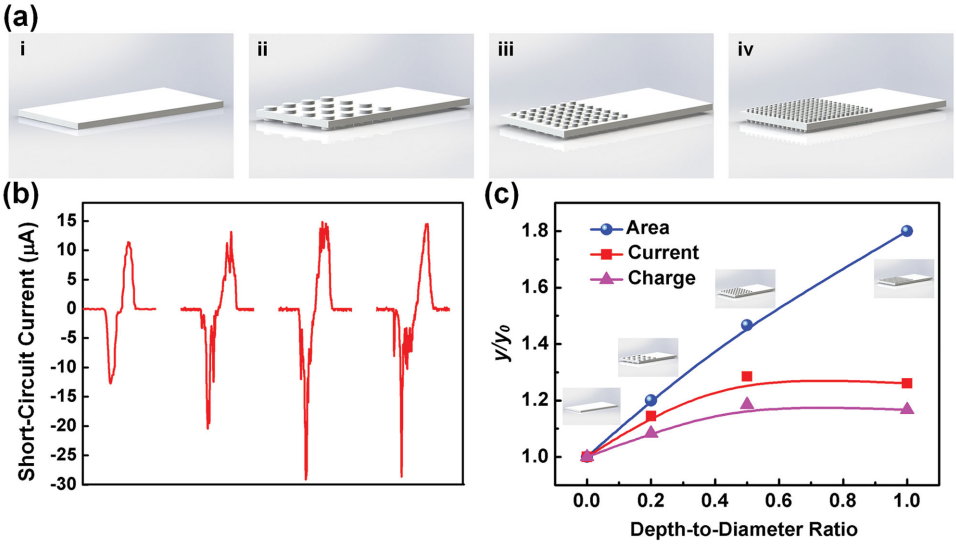

Figure 5. Dependences of the output performance of the LM-TENG on various surface morphologies. a) Schematic illustrations of the four kinds of surface morphologies. b) The short-circuit current for the four kinds of surface morphologies. c) Varying tendencies of the surface area, current, and transferred charges for the four kinds of surface morphologies (here y represents the value measured at each depth-to-diameter ratio and y_0 represents the value of the plane structure).

depth-to-diameter ratio approaches further higher, the amount of the electrons that can transport in one cycle saturates, and even drops a little. It is attributed to that mercury is not able to wet all the surface area on the sheet, although the specific surface area increases, which inevitably limits the generator's output.

2.5. Performance Enhancement by Layer Integration

The scalability of the LM-TENG's output in two dimensions is proved by changing the contacting area, as discussed above. Multilayer integration is thereby employed in the vertical direction to achieve multifold enhancement, which is previously reported to be very effective.[22] In this work, the liquid metal is continuously deformable, so that the experiment is performed expediently by stacking the slices together, as shown in **Figure 6**a.

Each slice is electrically connected with others in parallel. The equivalent circuit model is illustrated in Figure 6b. As the layer number increases from 1 to 20, the output current is significantly enhanced from 9 to 131 μA. Due to the uneven liquid metal level over all the slices, the achieved enhancement is not as high as 20 times bigger. As for the output voltage, it increases considerably and then saturates around 1400 V. It is owing to that the voltage meter in our experiment is similar to a load resistance. Therefore, with the increase of the current, the voltage value also increases to some degree.

2.6. Energy Conversion Efficiency of the LM-TENG

The efficiency of the LM-TENG is defined as the ratio between the input mechanical energy and the generated electric energy that is delivered to the load. When the slice is pushed down to the bottom of the liquid metal, the buoyancy and surface tension will force it to rise up. Under the action of the buoyancy, surface tension and its own weight (Figure S3, Supporting Information), the slice is accelerated to some speed and meanwhile delivers out the electric energy. Therefore, the efficiency is determined by the following equation

$$\eta = \frac{E_{ele}}{W_{total}} = \frac{\int I^2 R \, dt}{W_B + W_S - W_G} \quad (1)$$

where E_{ele} and W_{total} stand for the electric energy and the total work done by the ambient, and W_B, W_S, and W_G represent the work done by the buoyancy, surface tension, and gravity, respectively. E_{ele} is measured under various load resistances and shows an optimum energy output of 0.149 mJ at a load of 1 GΩ (**Figure 7**a,b). Whereas, the W_{total} is calculated to be 0.211 mJ (see Note 1 in the Supporting Information). Consequently, the efficiency reaches 70.6% at the best matched load (Figure 7c).

Such a high efficiency is attributed to the extremely low friction coefficient and large effective contacting surface of the liquid–solid contact. In addition, it is worth noting that, the slice is accelerated to some speed and thus possesses some kinetic energy. This is not dissipated during the energy generation process and should be excluded from the total input work. In our calculation, such a kinetic energy is ignored, which means that we underestimate the efficiency. The energy loss could be owing to that, during the surface tension's working process, the liquid requires inner motion and thus consumes some energy.

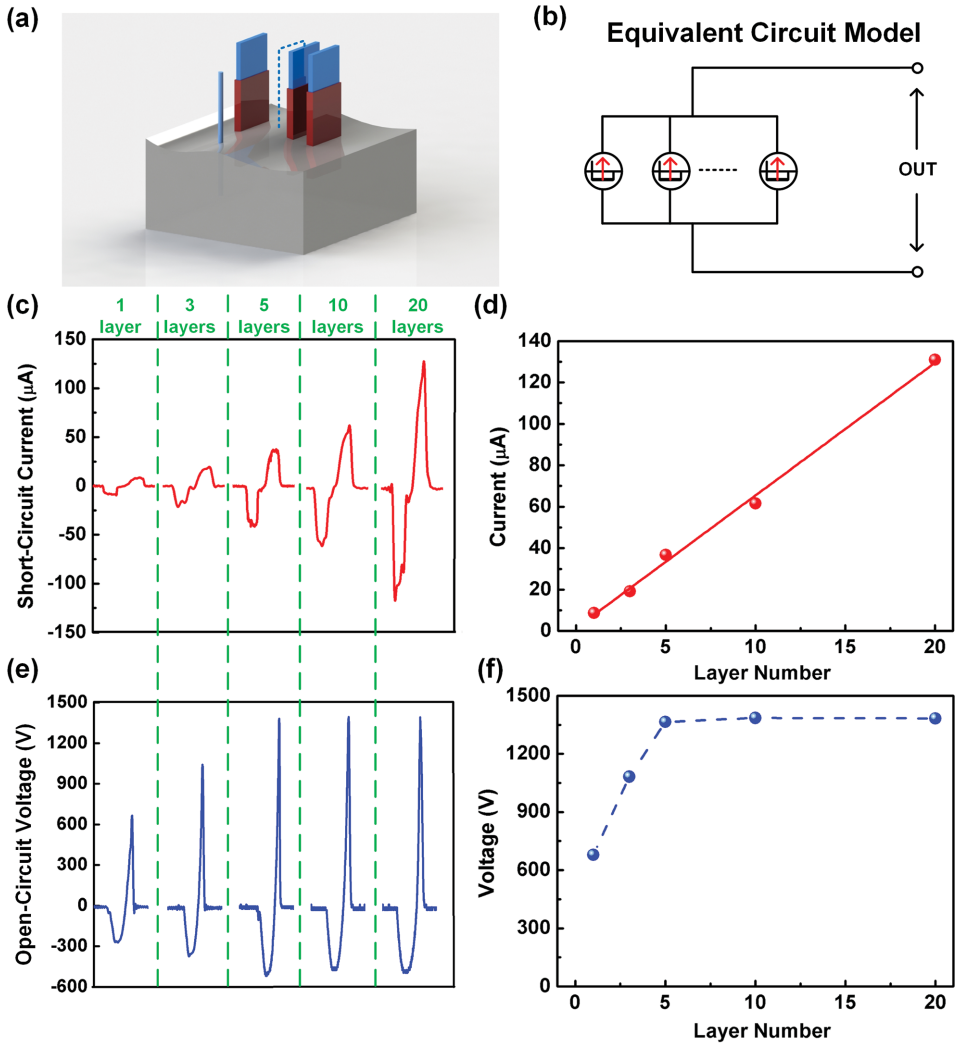

Figure 6. LM-TENG's output enhancement by layer integration. a) Schematic illustrations of the multilayered LM-TENG. b) The equivalent circuit model of the multilayered LM-TENG. c–f) Current and voltage enhancement with the increasing of the integrated layer number.

3. LM-TENG as a Power Source by Harvesting Human Motions and Ambient Vibrations

To demonstrate the capability of the LM-TENG as a power source, it is directly connected to hundreds of light-emitting diode (LED) bulbs. Driven by the hand motions, even very gentle, the LM-TENG can power up 150 LEDs (Video S1, Supporting Information).

Additionally, the liquid is normally easy fluctuating, which suggests an inherent technique of vibration energy harvesting. The configuration of the device is illustrated in **Figure 8**a. An acrylic box with 4 cm × 4 cm × 1.5 cm in size is fabricated to contain and seal the liquid metal, while ten slices are mounted in the box's lid, with their bottom ends suspended over the liquid level. Figure 8b shows the testing results of the device under various vibration frequencies with

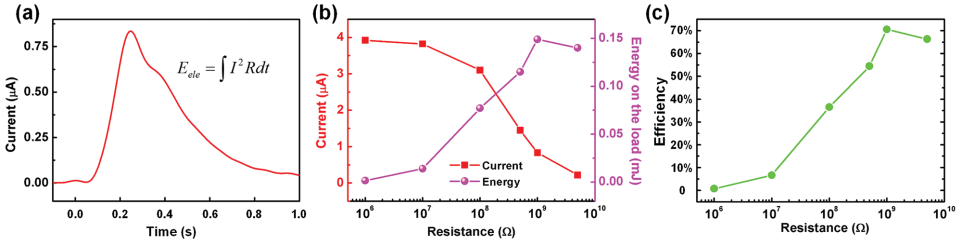

Figure 7. LM-TENG's energy efficiency measurement. a) Output current of the LM-TENG under free rising process at a load resistance of 1 GΩ. b) The output current and energy as a function of the load resistance. c) The energy efficiency of the LM-TENG at various load resistances.

DOI: 10.1002/adfm.201501331

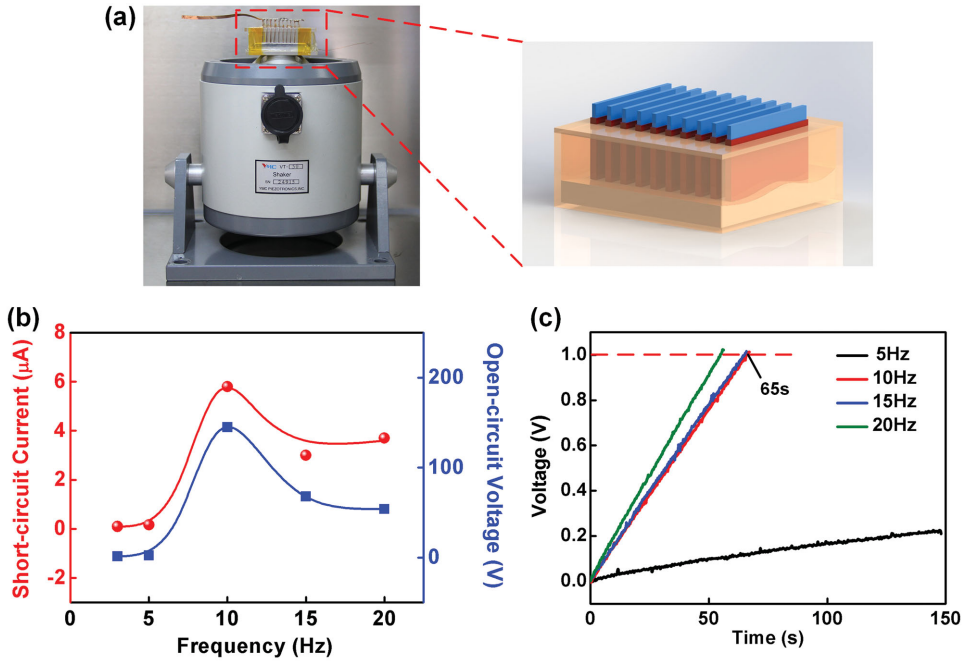

Figure 8. LM-TENG's application in the vibration energy harvesting. a) Schematic illustrations of the device and the testing setup. b) The output current and voltage as a function of the vibration frequency. c) The charging curves of a 100 μF capacitor under various vibration frequencies.

the amplitude of 1.2 mm. The maximum output current and voltage are 5.8 μA and 145 V, obtained at 10 Hz. With a bridge rectifier, the output charge without external load reaches 100 μC in 65 s (red line in Figure 8c). Video S2 (Supporting Information) shows the device powers up 150 LEDs under vibrations.

4. Conclusions

In summary, we develop the liquid-metal-based triboelectric nanogenerator. Owing to the outstanding properties of the liquid metal contact, such as enhanced effective contact, shape adaptability, and low friction coefficient with solid, the LM-TENG exhibits an output charge density of 430 μC m^{-2}, which is four to five times higher than that in the case if the electrode is solid film. With a 20-layer configuration, the LM-TENG achieves a high current output above 130 μA. In addition, the liquid-metal-based TENG's energy conversion efficiency is demonstrated to be 70.6% at the best matched load. Moreover, the easy-fluctuating property of the liquid metal makes it inherently suitable for vibration energy harvesting. Given its high output performance and other significant advantages in volume, scalability, the LM-TENG is a very promising approach in harvesting mechanical motions for self-powered electronics.

Supporting Information

Supporting Information is available from the Wiley Online Library or from the author.

Acknowledgements

W.T., T.J., and F.R.F. contributed equally to this work. Authors are thankful for the support from the "Thousands Talents" program for pioneer researcher and his innovation team, China, Beijing City Committee of Science and Technology projects (Z131100006013004), and the Beijing Natural Science Foundation of China (Grant No. 4141002) and the China Postdoctoral Science Foundation (Grant No. 2014M550031).

Received: April 2, 2015
Revised: April 16, 2015
Published online:

[1] Z. L. Wang, J. Song, *Science* **2006**, *312*, 242.
[2] R. Yang, Y. Qin, L. Dai, Z. L. Wang, *Nat. Nanotechnol.* **2008**, *4*, 34.
[3] S. Xu, Y. Qin, C. Xu, Y. Wei, R. Yang, Z. L. Wang, *Nat. Nanotechnol.* **2010**, *5*, 366.
[4] C. Chang, V. Tran, J. Wang, Y. Fuh, L. Lin, *Nano. Lett.* **2010**, *10*, 729.
[5] S. Beeby, R. Torah, *J. Micromech. Microeng.* **2007**, *17*, 1257.
[6] P. Glynne-Jones, M. Tudor, *Sens. Actuators, A* **2004**, *110*, 344.
[7] P. Mitcheson, P. Miao, B. Stark, *Sens. Actuators, A* **2004**, *115*, 523.
[8] Y. Naruse, N. Matsubara, *J. Micromech. Microeng.* **2009**, *19*, 1.
[9] H. O. Jacobs, G. M. Whitesides, *Science* **2001**, *291*, 1763.
[10] J. S. Boland, J. D. M. Messenger, H. W. Lo, Y. C. Tai, presented at the 18th Int. Conf. MEMS, CA, USA, Spring **2005**.
[11] T. Krupenkin, J. A. Taylor, *Nat. Commun.* **2011**, *2*, 448.
[12] J. K. Moon, J. Jeong, D. Lee, H. K. Pak, *Nat. Commun.* **2013**, *4*, 1487.
[13] H. T. Baytekin, A. Z. Patashinski, M. Branicki, B. Baytekin, S. Soh, B. A. Grzybowski, *Science* **2011**, *333*, 308.
[14] S. McCarty, G. M. Whitesides, *Angew. Chem. Int. Ed.* **2008**, *47*, 2188.
[15] F. Fan, Z. Tian, Z. L. Wang, *Nano Energy* **2012**, *1*, 328.
[16] Z. L. Wang, *ACS Nano* **2013**, *7*, 9533.
[17] X. Zhang, M. Han, R. Wang, F. Zhu, Z. Li, W. Wang, H. X. Zhang, *Nano Lett.* **2013**, *13*, 1168.

[18] L. Lin, Y. Xie, S. Niu, S. Wang, P. Yang, Z. L. Wang, *ACS Nano* **2015**, *9*, 922.
[19] G. Zhu, J. Chen, T. Zhang, Q. Jing, Z. L. Wang, *Nat. Commun.* **2014**, *5*, 3426.
[20] W. Tang, C. Han, C. Zhang, Z. L. Wang, *Nano Energy* **2014**, *9*, 121.
[21] L. Lin, S. Wang, Y. Xie, Q. Jing, S. Niu, Y. Hu, Z. L. Wang, *Nano Lett.* **2013**, *13*, 2916.
[22] W. Du, X. Han, L. Lin, M. Chen, X. Li, C. Pan, Z. L. Wang, *Adv. Energy Mater.* **2014**, *4*, 1301592.
[23] M. D. Dickey, R. C. Chiechi, R. J. Larsen, E. A. Weiss, D. A. Weitz, G. M. Whitesides, *Adv. Funct. Mater.* **2008**, *18*, 1097.
[24] S. Cheng, A. Rydberg, K. Hjort, Z. Wu, *Appl. Phys. Lett.* **2009**, *94*, 144103.
[25] Y. G. Deng, J. Liu, *Int. Commun. Heat Mass* **2010**, *37*, 788.
[26] J. So, J. Thelen, A. Qusba, G. J. Hayes, G. Lazzi, M. D. Dickey, *Adv. Funct. Mater.* **2009**, *19*, 3632.
[27] S. H. Jeong, A. Hagman, K. Hjort, M. Jobs, J. Sundgvist, Z. Wu, *Lab Chip* **2012**, *12*, 4657.
[28] K. Wang, K. Jiang, B. Chung, T. Ouchi, P. J. Burke, D. A. Boysen, D. J. Bradwell, H. Kim, U. Muecke, D. R. Sadoway, *Nature* **2014**, *514*, 348.
[29] Q. Zhang, J. Liu, *Nano Energy* **2013**, *2*, 863.
[30] C. B. Duke, T. J. Fabish, *J. Appl. Phys.* **1978**, *49*, 315.
[31] T. Liu, P. Sen, C. J. Kim, *J. Microelectromech. Syst.* **2012**, *21*, 443.
[32] G. Zhu, Y. Zhou, P. Bai, X. Meng, Q. Jing, J. Chen, Z. L. Wang, *Adv. Mater.* **2014**, *26*, 3788.
[33] C. Jeong, K. Baek, S. Niu, T. Nam, Y. Hur, D. Park, G. Hwang, M. Byun, Z. Wang, Y. Jung, K. Lee, *Nano Lett.* **2014**, *12*, 7031.

Adv. Funct. Mater. **2015**,
DOI: 10.1002/adfm.201501331